Structural Engineering and Mechanics, Vol. 5, No. 1 (1997) 85-104
DOI: http://dx.doi.org/10.12989/sem.1997.5.1.085

Effect of lateral restraint on the buckling behaviour of plates under non-uniform edge compression

Osama K. Bedair†

Civil Engineering Department, Concordia University, 1455 de Maisonneuve Blvd. W., Montreal, Quebec, H3G 1M8, Canada

Abstract. The paper investigates the influence of lateral restraint on the buckling behaviour of plate under non-uniform compression. The unloaded edges are assumed to be partially restrained against translation in the plane of the plate and the distributions of the resulting forces acting on the plate are shown. The stability analysis is done numerically using the Galerkin method and various strategies the economize the numerical implementation are presented. Results are obtained showing the variation of the buckling load, from free edge translation to fully restrained, with unloaded edges simply supported, clamped and partially restrained against rotation for various plate aspect ratios and stress gradient coefficients. An apparent decrease in the buckling load is observed due to these destabilizing forces acting in the plate and changes in the buckling modes are observed by increasing the intensity of the lateral restraint. A comparison is made between the buckling loads predicted from various formulas in stability standards based on free edge translation and the values derived from the present investigation. A difference of about 34% in the predicted buckling load and different buckling mode were found.

Key words: plate buckling; lateral restrain; Galerkin method.

1. Introduction

The traditional stability analysis of plates under combined compression and in-plane bending, is based on the assumption that the plate is free to move laterally and, hence, the restraints imposed by the attached elements against this motion are ignored. Such plates are encountered in webs of beam columns, channel sections, box sections under eccentric loading, stiffened plates, ...etc. The applied moment in this case causes the load to vary linearly in the transverse direction. The attached stiffeners or plate elements normally restrain the plate itself against both rotation and in-plane translation along the unloaded edges. The intensity of these restraints depends upon the geometric proportions of the plate and those of the attached elements. If, for example, the plate is attached to flange stiffener elements, as in the webs of I-sections, the torsional rigidity of the flanges determine the amount of rotational restraint and their cross sectional area determines the amount of lateral restraint and in-plane bending rigidity. The latter controls the freedom of the unloaded edges of the web to deform in-plane. Therefore, the stability analysis of plates requires three types of boundary conditions, namely; rotational, in-plane translation and bending of the unloaded edges. The first two are merely required for buckling analysis; however, all three are necessary to describe post-buckling.

† Ph. D.

The two extremes of rotational restraint are the rotationally free, (i.e. simply supported), and the rotationally clamped conditions. In the first case, the attached element is assumed to offer no resistance to rotation and the second case assumes that the attached element fully restrains the plate against rotation. The lateral restraint describes, on the other hand, the freedom of the unloaded edges to translate in-plane. If the plate is assumed to be free to translate (the classical assumption) the attached elements offer no resistance to this movement. If the plate is assumed to be fully restrained against lateral expansion the unloaded edges, in this case, are immoveable and destabilizing forces appear to lower the buckling stress. The third type of restraint describes the freedom of the unloaded edges to bend in the plane of the plate and, therefore, depends upon the in-plane bending rigidity of the attached element. In practice, the plate elements are partially restrained against rotation, in-plane translation and bending and, therefore, the buckling load and post-buckling stiffness fall between these limiting conditions.

Several expressions for the prediction of the buckling load of plates under compression and in-plane bending are available in design handbooks. Gaylord and Gaylord (1990) presented an approximate formula for the computation of the buckling coefficient for simply supported plates which forms the basis of the German specification, DIN4114, given by

$$K=\frac{8.4}{1.1+\Psi} \qquad \text{for } \beta\geq 1 \tag{1}$$

$$K=\frac{2.1}{1.1+\Psi}\left(\beta+\frac{1}{\beta}\right)^2 \qquad \text{for } \beta<1 \tag{2}$$

Where β is the plate aspect ratio and Ψ is the stress gradient coefficient. Beedle (1991) presented an alternative formula for the buckling coefficient of simply supported plates based on West European standard given by

$$K=\frac{16}{\sqrt{(1+\Psi)^2+0.112(1-\Psi)^2}+(1+\Psi)} \tag{3}$$

The Structural Stability Research Council, SSRC (Galambos 1988) presented numerical results for simply supported and clamped infinitely long plates.

It should be mentioned that expressions (1-3) are based on the assumption that the plate is free to translate in its plane and hence the lateral restraint imposed by the attached elements is ignored. To illustrate the influence of lateral restraints on the stability of plates under compression and in-plane bending, consider the plate shown in Fig. 1, compressed by a linearly varying load in the transverse direction. The distribution of the force is given by

$$N_x=N_1[(1-\Psi)\eta+\Psi] \tag{4}$$

where $\eta=y/b$.

If, in the analysis, the plate is considered to be laterally restrained against in-plane translation by the attached elements, a set of "interactive" forces, N_y and N_{xy}, appear due to this restraint having the distribution shown in Fig. 2. The normal force, N_y, varies linearly across the plate width and the shear forces are uniform along the loaded edges and vary linearly along the plate length. These distributions are obtained by solving the equilibrium equations

$$\frac{\partial N_x}{\partial \xi}+\beta\frac{\partial N_{xy}}{\partial \eta}=0 \tag{5}$$

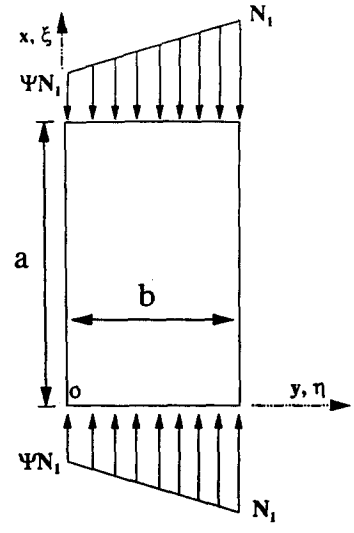

Fig. 1 Plate under combined compression and in-plane bending.

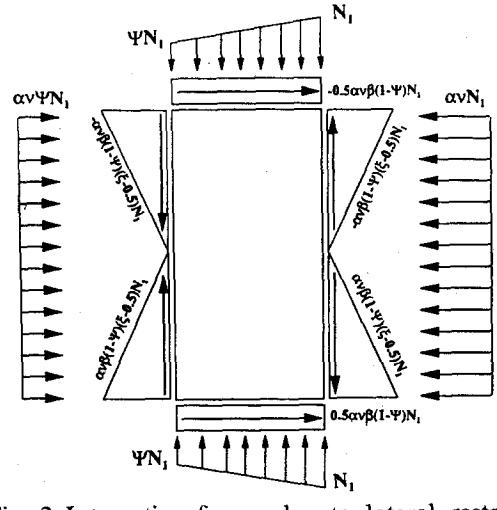

Fig. 2 Interactive forces due to lateral restraint.

$$\frac{\partial N_y}{\partial \xi}+\frac{1}{\beta}\frac{\partial N_{xy}}{\partial \eta}=0 \tag{6}$$

and are given by

$$N_y=\alpha \nu N_1\left[(1-\Psi)\,\eta+\Psi\right] \tag{7}$$

$$N_{xy}=-\alpha \nu N_1(1-\Psi)\,\beta\left(\xi-\frac{1}{2}\right) \tag{8}$$

where $\xi=x/a$. As shown in Fig. 2, the vertical shear force $(N_{xy})_{\eta=0}$ and $(N_{xy})_{\eta=1}$ are self equilibrated and the shear forces $(N_{xy})_{\xi=0}$ and $(N_{xy})_{\xi=1}$ are in equilibrium with the normal forces N_y. The

induced forces are function of Poisson's ratio (v), stress gradient (Ψ) and the lateral restraint coefficient $\alpha=(A/bt)/[1+(A/bt)]$, where A is the cross sectional area of the attached elements at $\eta=0, 1$, b and t are the width and thickness of the plate. Therefore, α varies from 0 (as $A/bt=0$) to 1 (as $(A/bt)\rightarrow\infty$). If the plate is free to translate in its own plane, the usual assumption of $\alpha=0$ eliminates these forces. This assumption is inherent in the analyses and in the expressions available in the literature (e.g., Schuette and Mculloch 1947, Johnson and Noel 1953, Bulson 1967, walker 1968, Rhodes and Harvey 1977, Maeda and Okura 1984, Usami 1982, Lau and Hancock 1986, Galambos 1988, Bradford 1989, Beedle 1991, and Okura, yen and Fisher 1993). If the plate is fully restrained against in-plane motion, α will have a value of unity. If the plate is uniformly compressed, i.e., $\Psi=1$, and orthogonally fully restrained, the shear forces disappear and the plate is under uniform bi-axial compression. The magnitude of the transverse force in this case $N_y=vN_1$. If the stress gradient, Ψ, equals zero, i.e., the applied force is triangular, the normal force $(N_y)_{\eta=0}$ disappears and $(N_y)_{\eta=1}$ is equilibrated by shear forces $(N_{xy})_{\xi=0}$ and $(N_{xy})_{\xi=1}$ only. The presence of these forces destabilizes the plate resulting in a lowered buckling stress and a possibly different buckling mode from the free motion case.

Previous papers Bedair (1996) investigate the buckling and post-buckling behaviour of plates under identical loading conditions. The in-plane boundary condition for the unloaded edges was free in-plane motion and the lateral restraint was not considered. The main objective of this paper is to snow the influence of lateral restraint on the buckling behaviour of plates under compression and in-plane bending. The Galerkin method is applied to evaluate numerically the buckling load of plates and results of plates with unloaded edges rotationally free, clamped and partially restrained against rotation are discussed. In addition, the reduction in the buckling load caused by the destabilizing forces is presented for various plate aspect ratios. These results show that the buckling mode might also be different from the usual assumption of free in-plane motion.

2. Theoretical analysis

The differential equation of this, elastic, isotropic plates subject to in-plane forces can be expressed in non-dimensional from as

$$\beta^{-2}\frac{\partial^4 w}{\partial\xi^4}+2\frac{\partial^4 w}{\partial\xi^2\partial\eta^2}+\beta^2\frac{\partial^4 w}{\partial\eta^4}=\frac{b^2}{D}\left[N_x\left(\frac{\partial^2 w}{\partial\xi^2}\right)+2\beta N_{xy}\left(\frac{\partial^2 w}{\partial\xi\partial\eta}\right)+\beta^2 N_y\left(\frac{\partial^2 w}{\partial\eta^2}\right)\right] \tag{9}$$

where β is the plate aspect ratio $=a/b$, D is the flexural rigidity $=Et^3/12(1-v^2)$, E is Young's modulus, v is Poisson's ratio and t is the plate thickness.

The out of plane displacement function can be expressed in separable form as

$$w_{mn}(\xi,\ \eta)=\sum_{m=1}^{N}\sum_{n=1}^{N} A_{mn}H_m(\xi)\,C_n(\eta) \tag{10}$$

where the functions $H_m(\xi)$ and $C_n(\eta)$ should satisfy the kinematic boundary conditions at $\xi=0$, 1 and $\eta=0$, 1, respectively. Using the Galerkin method, an approximate solution to Eq. (9) is obtained which results, after substituting from Eq. (10), in the following set of equations

$$\sum_{i=1}^{N}\sum_{j=1}^{N}\sum_{m=1}^{N}\sum_{n=1}^{N}\int_0^1\int_0^1\Big[\beta^{-2}H_m^{\text{IIII}}(\xi)\,C_n(\eta)+2H_m^{\text{II}}(\xi)C_n^{\cdot\cdot}(\eta)+\beta^2H_m(\xi)C_n^{\cdot\cdot\cdot\cdot}(\eta)$$

$$-\frac{b^2}{D}(N_xH_m^{\text{II}}(\xi)C_n(\eta)+2\beta N_{xy}H_m^{\text{I}}(\xi)C_n^{\cdot}(\eta)+\beta^2N_yH_mC_n^{\cdot\cdot})\Big] \tag{11}$$

$$H_i(\xi)\,C_j(\eta)\,d\xi d\eta=0$$

where the prime ($'$) and the dot ($\cdot$) denote differentiation with respect to ξ and η, respectively. Substituting Eqs. (4), (7), (8) into (11), the following eigenvalue problem is obtained

$$\sum_{i=1}^{N}\sum_{j=1}^{N}\sum_{m=1}^{N}\sum_{n=1}^{N}[Q_{mnij}-\lambda F_{mnij}]\,\boldsymbol{A_{mnij}}=0 \tag{12}$$

Where the Q_{mnij} is given by

$$[Q_{mnij}]=\int_0^1\int_0^1\Big(\beta^{-2}H_m^{\text{IIII}}(\xi)\,C_n(\eta)+2H_m^{\text{II}}(\xi)C_n^{\cdot\cdot}(\eta)+\beta^2H_m(\xi)C_n^{\cdot\cdot\cdot\cdot}(\eta)\Big)H_i(\xi)\,C_j(\eta)\,d\xi d\eta \tag{13}$$

and

$$\lambda=\frac{N_1b^2}{\pi^2D} \tag{14}$$

For convenience of the computational procedure, the force matrix F_{mnij} is partitioned into three sub-matrices, E_{mnij}, R_{mnij} and K_{mnij} such that

$$[F_{mnij}]=\pi^4[(1-\Psi)\,(E_{mnij}+2\alpha\nu\beta^2R_{mnij})+\Psi K_{mnij}] \tag{15}$$

where

$$[E_{mnij}]=-\frac{1}{\pi^2}\int_0^1\int_0^1\Big(H_m^{\text{II}}(\xi)\,C_n(\eta)+\alpha\nu\beta^2H_m(\xi C_n^{\cdot}(\eta)\Big)\,\eta H_i(\xi)\,C_j(\eta)\,d\xi d\eta \tag{16}$$

$$[R_{mnij}]=\frac{1}{\pi^2}\int_0^1\int_0^1\Big(\xi-\frac{1}{2}\Big)H_m^{\text{I}}(\xi)\,H_i(\xi)\,C_n^{\cdot}(\eta)\,C_j(\eta)d\xi d\eta \tag{17}$$

and

$$[K_{mnij}]=-\frac{1}{\pi^2}\int_0^1\int_0^1\Big(H_m^{\text{II}}(\xi)\,C_n(\eta)+\alpha\nu\beta^2H_m(\xi C_n^{\cdot\cdot}(\eta)\Big)H_i(\xi)\,C_j(\eta)\,d\xi d\eta \tag{18}$$

The sparsity of the $\boldsymbol{Q_{mnij}}$, $\boldsymbol{E_{mnij}}$, $\boldsymbol{R_{mnij}}$ and $\boldsymbol{K_{mnij}}$ matrices depends upon the assumed form of $H(\xi)$ and $C(\eta)$. In the following sections two boundary conditions for the unloaded edges are investigated, rotationally free and clamped. The loaded edges are treated in both cases as simply supported.

2.1. Rotationally free condition

The displacement functions $H_m(\xi)$ and $C_n(\eta)$ need to satisfy the following conditions

$$H_m(0)=H_m(1)=0,\quad H_m^{\text{II}}(0)=H_m^{\text{II}}(1)=0 \tag{19}$$

and

$$C_n(0)=C_n(1)=0, \quad C_n''(0)=C_n''(1)=0 \tag{20}$$

Choosing $H_m(\xi)$ and $C_n(\eta)$ of Eq. (10) as

$$H_m(\xi)=\sin(m\pi\xi), \quad C_n(\eta)=\sin(n\pi\eta) \tag{21}$$

and substituting Eq. (21) into Eq. (13), $\boldsymbol{Q}_{mnij}$ becomes

$$[Q_{mnij}]=\pi^4(\beta^{-2}m^4+2m^2n^2+\beta^2n^4)\int_0^1\int_0^1 \sin(m\pi\xi)\sin(i\pi\xi)\sin(n\pi\eta)\sin(j\pi\eta)\,d\xi d\eta \tag{22}$$

$$=\frac{\pi^4}{4}\left(\frac{m^2}{\beta}+\beta n^2\right)^2\delta_{mi}\delta_{nj} \tag{23}$$

where δ_{mi} is the kronecker delta defined as $\delta_{mi}=1$ if $m=i$ and zero otherwise. The E_{mnij} matrix of Eq. (16) is given by

$$[E_{mnji}]=(m^2+\alpha\nu\beta^2n^2)\int_0^1\int_0^1 \eta\sin(m\pi\xi)\sin(i\pi\xi)\sin(n\pi\eta)\sin(j\pi\eta)\,d\xi d\eta \tag{24}$$

$$=\frac{1}{8}(m^2+\alpha\nu\beta^2n^2)\,\delta_{mi}\delta_{nj} \tag{25}$$

$$=-\frac{2}{\pi^2}(m^2+\alpha\nu\beta^2n^2)\,\delta_{mi}\frac{nj}{(j^2-n^2)^2} \qquad \text{if } n+j \text{ odd} \tag{26}$$

$$=0 \text{ elsewhere} \tag{27}$$

R_{mnij} is given by

$$[R_{mnij}]=mn\int_0^1\int_0^1\left(\xi-\frac{1}{2}\right)\cos(m\pi\xi)\sin(i\pi\xi)\cos(n\pi\eta)\sin(j\pi\eta)\,d\xi d\eta \tag{28}$$

$$=\frac{2}{\pi^2}\frac{mnij}{(m^2-i^2)(j^2-n^2)} \qquad \text{if } m+i \text{ even, } m\neq i,\ n+j \text{ odd} \tag{29}$$

$$=-\frac{1}{2\pi^2}\frac{nj}{j^2-n^2}\,\delta_{mi} \qquad \text{if } n+j \text{ odd} \tag{30}$$

$$=0 \qquad \text{elsewere} \tag{31}$$

Finally, $\boldsymbol{K}_{mnij}$ is given by

$$[K_{mnij}]=(m^2+\alpha\nu\beta^2n^2)\int_0^1\int_0^1 \sin(m\pi\xi)\sin(i\pi\xi)\sin(n\pi\eta)\sin(j\pi\eta)\,d\xi d\eta \tag{32}$$

$$=\frac{1}{4}(m^2+\alpha\nu\beta^2n^2)\,\delta_{mi}\delta_{nj} \quad \text{if } m+i \text{ odd, } n+j \text{ odd} \tag{33}$$

$$=0 \quad \text{elsewhere} \tag{34}$$

2.1.2. Computational procedure

The solution of the eigen-value defined by Eq. (12) requires the evaluation of five matrices

each of order $(m\times n)\times(i\times j)$. To illustrate the properties of these matrices that can be taken into account in the computational procedure, consider a typical matrix $[\boldsymbol{B}]$, which may represent any of $\boldsymbol{Q}_{mnij}$, $\boldsymbol{E}_{mnij}$, $\boldsymbol{K}_{mnij}$ or $\boldsymbol{R}_{mnij}$, partitioned, by fixing m and i and varying n and j into the following system of sub-matrices

$$
[\boldsymbol{B}]=\begin{bmatrix}
\begin{bmatrix} b_{1111} & b_{1211} & \cdots & b_{1n11} \\ b_{1112} & b_{1212} & \cdots & b_{1n12} \\ b_{1113} & b_{1213} & \cdots & b_{1n13} \\ \cdot & \cdot & \cdots & \cdot \\ \cdot & \cdot & \cdots & \cdot \\ b_{111j} & b_{121j} & \cdots & b_{1n1j} \end{bmatrix} & \begin{bmatrix} b_{2111} & b_{2211} & \cdots & b_{2n11} \\ b_{2112} & b_{2212} & \cdots & b_{2n12} \\ b_{2113} & b_{2213} & \cdots & b_{2n13} \\ \cdot & \cdot & \cdots & \cdot \\ \cdot & \cdot & \cdots & \cdot \\ b_{211j} & b_{221j} & \cdots & b_{2n1j} \end{bmatrix} & \cdots & \begin{bmatrix} b_{m111} & b_{m211} & \cdots & b_{mn11} \\ b_{m112} & b_{m212} & \cdots & b_{mn12} \\ b_{m113} & b_{m213} & \cdots & b_{mn13} \\ \cdot & \cdot & \cdots & \cdot \\ \cdot & \cdot & \cdots & \cdot \\ b_{m11j} & b_{m21j} & \cdots & b_{mn1j} \end{bmatrix} \\
\begin{bmatrix} b_{1121} & b_{1221} & \cdots & b_{1n21} \\ b_{1122} & b_{1222} & \cdots & b_{1n22} \\ b_{1123} & b_{1223} & \cdots & b_{1n23} \\ \cdot & \cdot & \cdots & \cdot \\ \cdot & \cdot & \cdots & \cdot \\ b_{112j} & b_{122j} & \cdots & b_{1n2j} \end{bmatrix} & \begin{bmatrix} b_{2121} & b_{2221} & \cdots & b_{2n21} \\ b_{2122} & b_{2222} & \cdots & b_{2n22} \\ b_{2123} & b_{2223} & \cdots & b_{2n23} \\ \cdot & \cdot & \cdots & \cdot \\ \cdot & \cdot & \cdots & \cdot \\ b_{212j} & b_{222j} & \cdots & b_{2n2j} \end{bmatrix} & \cdots & \begin{bmatrix} b_{m121} & b_{m221} & \cdots & b_{mn21} \\ b_{m122} & b_{m222} & \cdots & b_{mn22} \\ b_{m123} & b_{m223} & \cdots & b_{mn23} \\ \cdot & \cdot & \cdots & \cdot \\ \cdot & \cdot & \cdots & \cdot \\ b_{m12j} & b_{m22j} & \cdots & b_{mn2j} \end{bmatrix} \\
\vdots & \vdots & \cdots & \vdots \\
\begin{bmatrix} b_{11i1} & b_{12i1} & \cdots & b_{1ni1} \\ b_{11i2} & b_{12i2} & \cdots & b_{1ni2} \\ b_{11i3} & b_{12i3} & \cdots & b_{1ni3} \\ \cdot & \cdot & \cdots & \cdot \\ \cdot & \cdot & \cdots & \cdot \\ b_{11ij} & b_{12ij} & \cdots & b_{1nij} \end{bmatrix} & \begin{bmatrix} b_{21i1} & b_{22i1} & \cdots & b_{2ni1} \\ b_{21i2} & b_{22i2} & \cdots & b_{2ni2} \\ b_{21i3} & b_{22i3} & \cdots & b_{2ni3} \\ \cdot & \cdot & \cdots & \cdot \\ \cdot & \cdot & \cdots & \cdot \\ b_{21ij} & b_{22ij} & \cdots & b_{2nij} \end{bmatrix} & \cdots & \begin{bmatrix} b_{m1i1} & b_{m2i1} & \cdots & b_{mni1} \\ b_{m1i2} & b_{m2i2} & \cdots & b_{mni2} \\ b_{m1i3} & b_{m2i3} & \cdots & b_{mni3} \\ \cdot & \cdot & \cdots & \cdot \\ \cdot & \cdot & \cdots & \cdot \\ b_{m1ij} & b_{m2ij} & \cdots & b_{mnij} \end{bmatrix}
\end{bmatrix} \tag{35}
$$

Each of the sub-matrices is of order $(n\times j)$, (n and $j=1, 2, \cdots, N$). Note that n varies through the columns and j through the rows. The matrix $[\boldsymbol{B}]$ can be written in compact from as

$$
\boldsymbol{B}=\begin{bmatrix}
[\boldsymbol{B}_{1n1j}] & [\boldsymbol{B}_{2n1j}] & [\boldsymbol{B}_{3n1j}] & \cdots & [\boldsymbol{B}_{mn1j}] \\
[\boldsymbol{B}_{1n2j}] & [\boldsymbol{B}_{2n2j}] & [\boldsymbol{B}_{3n2j}] & \cdots & [\boldsymbol{B}_{mn2j}] \\
[\boldsymbol{B}_{1n3j}] & [\boldsymbol{B}_{2n3j}] & [\boldsymbol{B}_{3n3j}] & \cdots & [\boldsymbol{B}_{mn3j}] \\
\cdot & \cdot & \cdot & \cdots & \cdot \\
\cdot & \cdot & \cdot & \cdots & \cdot \\
[\boldsymbol{B}_{1nij}] & [\boldsymbol{B}_{2nij}] & [\boldsymbol{B}_{3nij}] & \cdots & [\boldsymbol{B}_{mnij}]
\end{bmatrix} \tag{36}
$$

The evaluation of $\boldsymbol{Q}_{mnij}$ and $\boldsymbol{K}_{mnij}$ requires only the computation of the diagonal terms of these matrices, i.e., b_{1111}, b_{1212}, b_{1313}, $\cdots$, b_{mnij} (for $i=m$ and $n=j$), of the B matrix as shown schematically in Fig. (3). It can be observed that the $\boldsymbol{K}_{mnij}$ matrix is a function of β and α which are variable parameters for each eigen-value problem. A convenient automation process is to first generate a diagonal matrix with diagonal terms of 1/4. By inputting β and α, modification factors $(m^2+\alpha\nu\beta^2 n^2)$ are calculated and multiplied by the associated entries. Because of the partitioning scheme used, each sub-matrix will have a constant m and a variable n. For example, if $\beta=2$, $\nu=0.3$ and $\alpha=0.5$ the modification factors for $\{\boldsymbol{B}_{1n1j}, \boldsymbol{B}_{2n2j}, \boldsymbol{B}_{3n3j}\}$ are $\{(1+0.6n^2), (4+0.6\ n^2), (9+0.6\ n^2)\}$, respectively.

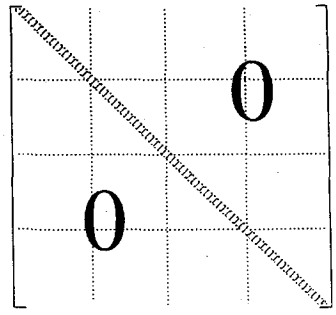

Fig. 3 Property of Q_{mnij} matrix.

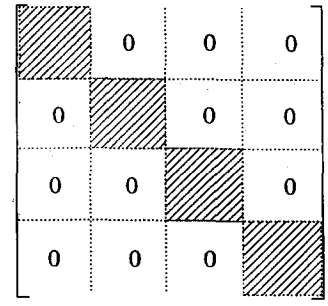

Fig. 4 Property of E_{mnij} matrix.

The generation of E_{mnij} requires only the computation of the diagonal sub-matrices, B_{1n1j}, B_{2n2j}, $\cdots$, B_{mnij} (for $m=i$), shown by the shaded area in Fig. (4). The remaining sub-matrices are zero. The matrix is also a function of β and α; therefore, a convenient way is to generate first a "basic" sub-matrix, B^0, containing the following entries

$$[\boldsymbol{B}^0]=\frac{\delta_{nj}}{8} \tag{37}$$

$$=-\frac{2}{\pi^2}\frac{nj}{(j^2-n^2)^2} \quad \text{if } n+j \text{ odd} \tag{38}$$

where the first and the second equations represent the diagonal and off diagonal entries, respectively, of the sub-matrix. Note also that the sub-matrix is symmetric about the diagonal. Because of the partitioning scheme used, all the diagonal sub-matrices of the assembled basic matrix $[B^b]$ are identical and need not be re-generated, i.e.

$$[\boldsymbol{B}^b]=\begin{bmatrix} [\boldsymbol{B}^0] & [\mathbf{0}] & [\mathbf{0}] & \cdots & [\mathbf{0}] \\ [\mathbf{0}] & [\boldsymbol{B}^0] & [\mathbf{0}] & \cdots & [\mathbf{0}] \\ [\mathbf{0}] & [\mathbf{0}] & [\boldsymbol{B}^0] & \cdots & [\mathbf{0}] \\ \cdot & \cdot & \cdot & \cdots & \cdot \\ \cdot & \cdot & \cdot & \cdots & \cdot \\ [\mathbf{0}] & [\mathbf{0}] & [\mathbf{0}] & \cdots & [\boldsymbol{B}^0] \end{bmatrix} \tag{39}$$

Then, for a given β an α, the modification factors $(m^2+\alpha\nu\beta^2n^2)$ are computed and multiplied by the corresponding sub-matrix, as illustrated for the computation of the $\boldsymbol{K}_{mnij}$ matrix.

A similar procedure can be followed to generate $\boldsymbol{R}_{mnij}$. The basic sub-matrix, B^0, in this case is given by

$$[B^0]=-\frac{2}{\pi^2}\frac{nj}{(j^2-n^2)} \quad \text{if } n+j \text{ odd} \tag{40}$$

$$=0 \quad \text{elsewere} \tag{41}$$

and the modification factors for the sub-matrices are

$$MF^1=\frac{mi}{i^2-m^2} \quad \text{if } m+i \text{ even}, \ m\neq i \tag{42}$$

$$MF^2=\frac{1}{4} \qquad \text{if } m=i \tag{43}$$

The diagonal sub-matrices are all multiplied by a factor of 1/4 and sub-matrices of $m+i$=even are multiplied by MF^1, i.e.

$$\boldsymbol{R}_{mnij}=\begin{bmatrix} MF^2[\boldsymbol{B}^0] & [\boldsymbol{0}] & MF^1[\boldsymbol{B}^0] & \cdots & MF^k[\boldsymbol{B}^0] \\ [\boldsymbol{0}] & MF^2[\boldsymbol{B}^0] & [\boldsymbol{0}] & \cdots & MF^k[\boldsymbol{B}^0] \\ MF^1[\boldsymbol{B}^0] & [\boldsymbol{0}] & MF^2[\boldsymbol{B}^0] & \cdots & MF^k[\boldsymbol{B}^0] \\ \cdot & \cdot & \cdot & \cdots & \cdot \\ \cdot & \cdot & \cdot & \cdots & \cdot \\ MF^k[\boldsymbol{B}^0] & MF^k[\boldsymbol{B}^0] & MF^k[\boldsymbol{B}^0] & \cdots & MF^2[\boldsymbol{B}^0] \end{bmatrix} \tag{44}$$

where MF^k ($k=1$ or 2) depends upon the number of m and i chosen in the truncated series, noting that, if $m+i$ is odd, the sub-matrix is zero and does not need to be generated.

2.2. Clamped-clamped condition

The unloaded edges in this case need to satisfy the zero deflection and slope conditions;

$$C_n(0)=C_n(1)=0,\ C_n'(0)=C_n'(1)=0 \tag{45}$$

and the loaded edges satisfy the conditions given by Eqs. (19). A set of displacement functions that satisfy these conditions is assumed to be

$$H_m(\xi)=\sin(m\pi\xi),\ C_n(\eta)=\sin^2(n\pi\eta) \tag{46}$$

Substituting these functions into Eq. (13), the Q_{mnij} matrix is given by

$$[Q_{mnij}]=\pi^4\int_0^1\int_0^1[\beta^{-2}m^4\sin^2(n\pi\eta)\sin^2(j\pi\eta)-4(n^2m^2+2\beta^2n^4)\cos(2n\pi\eta)\sin^2(n\pi\eta)]$$
$$\sin(m\pi\xi)\sin(i\pi\xi)\,d\xi\,d\eta \tag{47}$$

$$=\frac{\pi^4}{2}(\beta^{-2}m^4\theta_{nj}+(m^2n^2+2n^4\beta^2)\,\delta_{nj})\,\delta_{mi} \tag{48}$$

where θ_{nj} is given by

$$\theta_{nj}=\frac{3}{8}\,\delta_{nj} \tag{49}$$

$$=\frac{1}{4} \qquad \text{if } n\neq j \tag{50}$$

The components of the force matrices, $\boldsymbol{E}_{mnij}$, $\boldsymbol{R}_{mnji}$ and $\boldsymbol{K}_{mnji}$ of Eq. (15) are obtained by substituting Eqs. (21) into (16)-(18)

$$[E_{mnij}]=\int_0^1\int_0^1\eta\,[m^2\sin^2(n\pi\eta)-2\alpha\nu\beta^2n^2\cos(2n\pi\eta)]\sin^2(j\pi\eta)\sin(m\pi\xi)\sin(i\pi\xi)\,d\xi\,d\eta \tag{51}$$

$$=\frac{1}{4}\left(m^2\theta_{nj}+\frac{1}{2}\alpha\nu\beta^2n^2\delta_{nj}\right)\delta_{mi} \tag{52}$$

$$[R_{mnij}]=\pi^2 mn\int_0^1\int_0^1\left(\xi-\frac{1}{2}\right)\cos(m\pi\xi)\sin(i\pi\xi)\sin(2\pi\eta)\sin^2(j\pi\eta)\,d\xi d\eta \tag{53}$$

$$=0 \tag{54}$$

$$[K_{mnij}]=\int_0^1\int_0^1[m^2\sin^2(n\pi\eta)-2\alpha\nu\beta^2n^2\cos(2n\pi\eta)]\sin^2(j\pi\eta)\sin(m\pi\xi)\sin(i\pi\xi)\,d\xi d\eta \tag{55}$$

$$=\frac{1}{2}\left(m^2\theta_{nj}+\frac{1}{2}\alpha\nu\beta^2n^2\delta_{nj}\right)\delta_{mi} \tag{56}$$

Combining Eqs. (52, 54, 56), the force matrix $\boldsymbol{F}_{mnij}$ becomes

$$[F_{mnij}]=\frac{\pi^4}{2}(1+\Psi)\left(m^2\theta_{nj}+\frac{1}{2}\alpha\nu\beta^2n^2\delta_{nj}\right)\delta_{mi} \tag{57}$$

2.2.1. Computational procedure

In this case, the diagonal sub-matrices of $\boldsymbol{Q}_{mnij}$ are the only non-zero ones. The diagonal entries of the sub-matrices are given by

$$b_{mnij}=\frac{1}{2}\left[\frac{3}{8}\frac{m^4}{\beta^2}+m^2n^2+2n^4\beta^2\right]\qquad \text{for } m=i,\ n=j \tag{58}$$

and the off diagonal terms are given by

$$b_{mnji}=\frac{1}{8}\frac{m^4}{\beta^2}\qquad \text{for } m=i \tag{59}$$

Since each sub-matrix contains a fixed m value, all the off diagonal terms of the sub-matrix are equal and the off-diagonal terms are variable. If, for example, $\beta=2$, B_{2n1j} is given by

$$[\boldsymbol{B}_{2nij}]=\begin{bmatrix} \frac{27}{4} & \frac{1}{2} & \frac{1}{2} & \cdots & \frac{1}{2} \\ \frac{1}{2} & \frac{291}{4} & \frac{1}{2} & & \frac{1}{2} \\ \cdot & \cdot & \cdot & \cdots & \cdot \\ \cdot & \cdot & \cdot & \cdots & \cdot \\ \frac{1}{2} & \frac{1}{2} & \frac{1}{2} & \cdots & \left(\frac{3}{4}2n^2(1+2n^2)\right) \end{bmatrix} \tag{60}$$

The force matrix, $\boldsymbol{F}_{mnij}$, also possesses a similar property, being diagonal and having identical off-diagonal terms in the sub-matrices. The diagonal terms of the matrix in this case are given by

$$b_{mnij}=\frac{(1+\Psi)}{4}\left[\frac{3}{8}m^2+\frac{1}{2}\alpha\nu\beta^2n^2\right]\qquad \text{for } m=i,\ n=j \tag{61}$$

and the off-diagonal terms of the diagonal sub-matrices are given by

$$b_{mnij}=\frac{1}{16}m^2(1+\Psi) \qquad \text{for } m=i \tag{62}$$

Note that only the diagonal terms are functions of β and α. A convenient way to generate the matrix is to generate a basic sub-matrix with diagonal terms equal to 1/4 and off-diagonal terms equal to 1/16. For given values of β, α and Ψ, modification factors of $m^2(1+\Psi)$ for the off-diagonal terms and $(1+\Psi)(0.735m^2+0.5\alpha\nu\beta^2n^2)$ for the diagonal terms are computed and pre-multiplied by the proper sub-matrix.

3. Numerical results

Computer programs were developed to investigate the buckling behaviour of the plate stress gradient. In all cases Poission's ratio was taken to be 1/3. The structure of the program for the simply supported case is shown in Fig. (5) and the basic components are summarized as follows;

(1) Input data are the plate aspect ratio (β) the initial values of the lateral restraint (α^0), the stress gradient coefficients (Ψ^0) and their increments (I and L) and number of increments (II and LL). If only one value of α and Ψ need to be analyzed, II and LL should be set equal to 1.

(2) Generate the diagonal entries of the $\boldsymbol{Q}_{mnij}$ matrix.

(3) Generate the basic sub-matrices of $\boldsymbol{K}_{mnij}$, $\boldsymbol{E}_{mnij}$ and $\boldsymbol{R}_{mnij}$ of the force matrix.

(4) Compute the modification factors for the given β, α, and Ψ and pre-multiply them by the corresponding sub-matrices in the assembled $\boldsymbol{K}_{mnij}$, $\boldsymbol{E}_{mnij}$ and $\boldsymbol{R}_{mnij}$ matrices.

(5) Solve the resulting eigen value problem to obtain the buckling load and its associated mode.

(6) Increase α by the prescribed I increment II times.

(7) Go to step (4)

(8) Increase Ψ by the prescribed L increment LL times.

(9) Go to step (4)

In the case of the clamped condition, the numerical algorithm is very similar; however, in stage (2) the diagonal sub-matrices are generated for the $\boldsymbol{Q}_{mnij}$ matrix, instead, and the load sub-matrix is generated in one stage.

The programs were verified for the simply supported and clamped conditions for the free in-plane translation ($\alpha=0$) condition. A comparison is made in Table 1 with the numerical results available in Bulson 1967, Column Research Committee of Japan (1971). The upper part of the table compares the simply supported case with numerical values reported in Bulson (1976). The lower part is a comparison of numerical values obtained for the clamped condition with values available in Column Research Committee of Japan (1971). As can be seen they are both in close agreement.

3.1. Simply supported condition

Results are presented for this boundary condition for three aspect ratios, $\beta=1$, 2 and 3. Sixteen

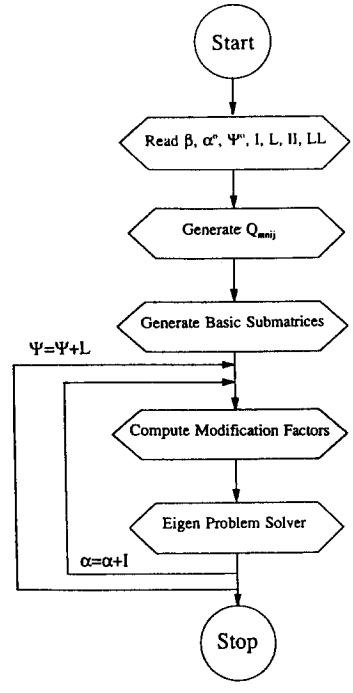

Fig. 5 Flow chart of numerical algorithm.

terms of the series were chosen. For a fixed value of Ψ, the initial value of $\alpha=0$ was chosen and an increment of 0.05 was selected to find the buckling load and the associated buckling mode for the full range of α from 0-1. The increments in Ψ were variable for some aspect ratios.

Fig. 6 shows the variation of the buckling load factor, K, with the lateral restraint coefficient, α, for $\beta=1$ and $\Psi=0$, 0.2, 0.4, 0.8, 1. The plate buckles into single half-sine waves for all values of stress gradient Ψ. As can be observed, a pronounced reduction in the buckling coefficient, K, results by increasing the lateral restraint coefficient, α, from 0 to 1. Typically, the K value, for example, reduces by almost 27% from the free translation case, $\alpha=0$, to the fully restrained situation, $\alpha=1$, for $\Psi=0$. Similar behaviour is observed for other values of Ψ. For example, a reduction by 26%, 25.5%, 25.6%, 25%, for $\Psi=0.2$, 0.4, 0.8, 1, respectively, is attained when α varies from 0 to 1.

Figs. 7 and 8 show the variation of K and α for other aspect ratios, $\beta=2$ and 3. The solid triangles represent the bimodal points. For $\beta=2$, Fig. 7, the plate changes its buckling mode from a full-sine wave to a half-sine wave at $\alpha=0.73$. In Fig. 8, the buckling mode changes from three half sine-waves to a full-sine wave at $\alpha\approx0.5$. For these aspect ratios, the reduction in the buckling load by changing α from 0 to 1 was within 39%~33%, showing the importance of defining the in-plane boundary condition for the prediction of the buckling load of the plate.

Table 2 shows a comparison between the predictions of the buckling coefficient, K with the German specification, DIN4114, Eq. (2), as presented by Gaylord, E. H and Gaylord, C.N. (1990),

Table 1 Numerical verification of K for simply supported and clamped conditions, for $\alpha=0$

Ψ	β	Refs. [10, 16]	Present
a) Simply supported Condition			
−1	1	25.6	25.5
−1/3		11	11.01
0		7.8	7.81
1/5		6.6	6.59
1/3		5.8	5.9
1		4	4
−1	1.5	24.1	24.1
−1/3		11.5	11.48
0		8.4	8.37
1/5		7.1	7.11
1/3		6.1	6.3
b) Rotationally clamped condition			
0	0.7	13.7	13.9
	0.8	14.3	14.2
	1	15	15.2
1	1	7.7	7.69
	2	7	6.99

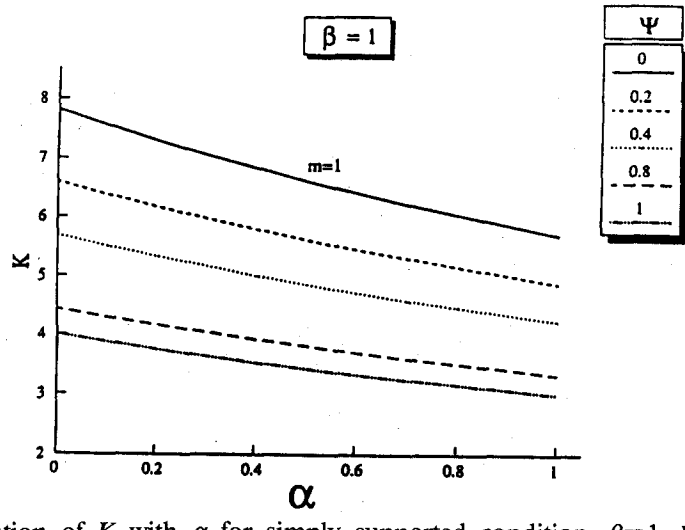

Fig. 6 Variation of K with α for simply supported condition, $\beta=1$, Ψ is variable.

and the expression presented by Beedle (1991) and given by Eq. (3) for plate aspect ratio, $\beta=4$. Noting that all these cases involve free translation, $\alpha=0$. The fourth and fifth columns of the table show the numerical predictions obtained from the present investigation for the free and fully restrained condition, $\alpha=0$ and 1, respectively, for $\Psi=0.4$, 0.6, 0.8. The quantity in the brackets representing the number of half-sine waves in the buckling mode. As can be seen, the numerical values for $\alpha=0$, are in good agreements with the values of Gaylord, E. H. Gaylord, C. N. (1990),

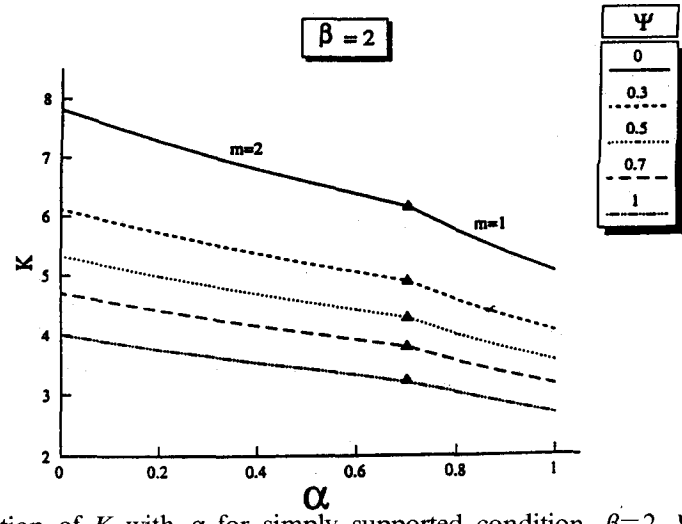

Fig. 7 Variation of K with α for simply supported condition, $\beta=2$, Ψ is variable.

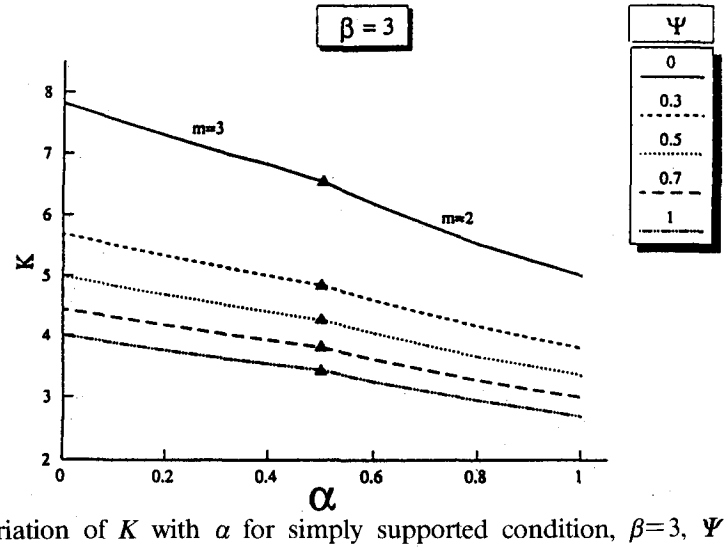

Fig. 8 Variation of K with α for simply supported condition, $\beta=3$, Ψ is variable.

Beedle (1991). The numerical values for $\alpha=1$, on the other hand, is less by 34% for $\Psi=0.4$, by 33.3% for $\Psi=0.6$ and by 33.1% for $\Psi=0.3$. The predicted buckling modes also differ indicating that these code expressions are valid only in the case of free edge translation. They seriously overestimate the buckling load if the plate in restrained against this motion.

3.2. Clamped-clamped condition

The variation of buckling coefficient, K with lateral restraint coefficient, α and $\beta=1$, 3, 5 under various stress gradients Ψ for the clamped condition are shown in Figs. 9,10 and 11. For $\beta=1$, Fig. 9, the buckling mode changes from a full-sine wave to a half-sine wave at α 0.35 for all Ψ. The average decrease in K by increasing α from 0 to 1 is about 20%. For $\beta=3$, Fig. 10, the plate buckling mode changes from $m=5$ to $m=4$ at $\alpha\approx0.07$ and the average reduction

Table 2 Comparison of K for free translation and fully restrained condition

Ψ	DIN 4114 (1990)	Beedle (1991)	Numerical ($\alpha=0$)	Numerical ($\alpha=1$)
0.4	5.6 (4)	5.68 (4)	5.71 (4)	3.75 (4)
0.6	4.94 (4)	4.99 (4)	5 (4)	3.33 (2)
0.8	4.42 (4)	4.44 (4)	4.44 (4)	2.97 (2)
1	4 (4)	4 (4)	4 (4)	2.7 (2)

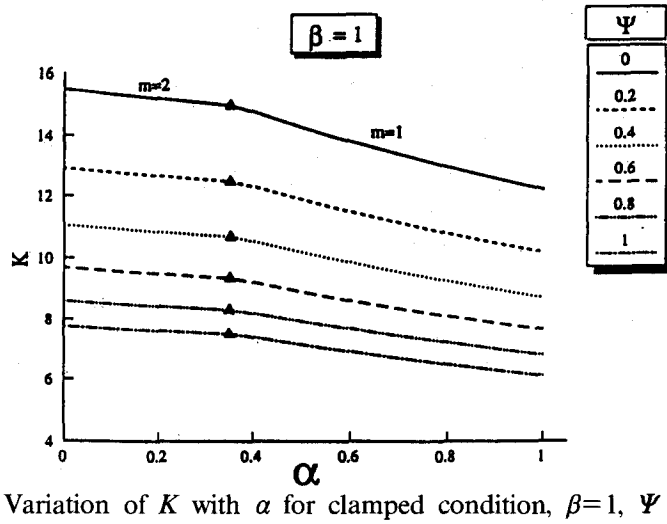

Fig. 9 Variation of K with α for clamped condition, $\beta=1$, Ψ is variable.

in K is about 18%. For $\beta=5$, Fig. 11, the changes in the buckling mode is from four sine waves to seven half-sine waves at $\alpha\approx0.94$. The average reduction in K is about 17.5%.

3.3. Partially restrained against rotation boundary condition

The previous sections showed the influence of lateral restraints for the limiting conditions of plates simply supported and clamped boundaries. In this section, the investigation is extended to show the influence of this restraint for the general case of unloaded edges partially restrained against rotation. Introducing Γ as the rotational restraint coefficient that varies from 0 (simply supported condition) to ∞ (rotationally clamped condition), the variable parameters now are the stress gradient coefficient (Ψ), strategy for the graphical presentation, is to fix β and Ψ and show the variation of the buckling coefficient, K, versus Γ, and various lateral restraints, α. To illustrate this effect, a schematic is shown in Fig. 12. Usually by increasing Γ, the change of the buckling mode, if it happens, is upward, i.e., from mode (i) to ($i+1$) to ($i+2$) ··· etc.

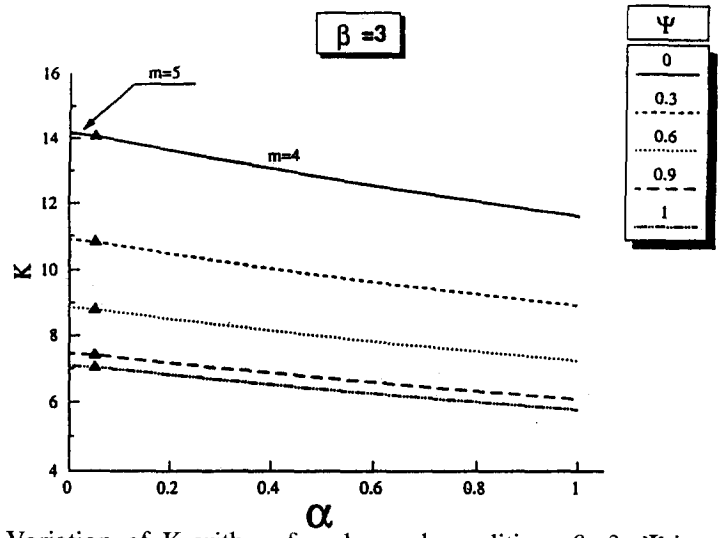

Fig. 10 Variation of K with α for clamped condition, $\beta=3$, Ψ is variable.

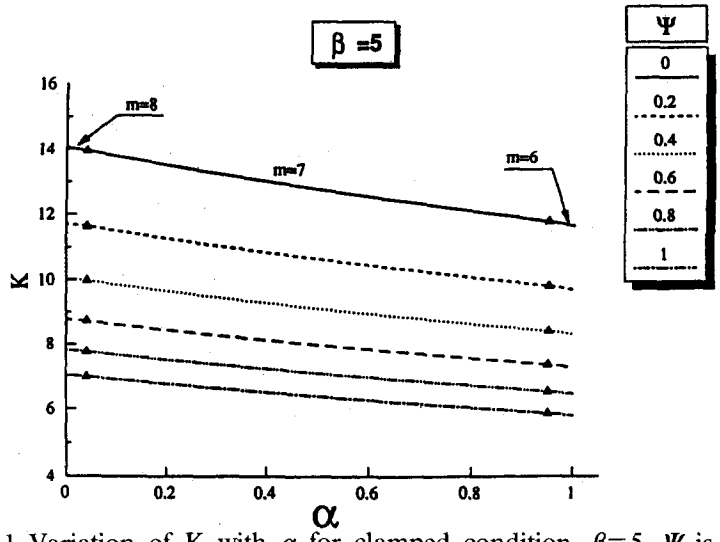

Fig. 11 Variation of K with α for clamped condition, $\beta=5$, Ψ is variable.

To maintain clarity of the curves, only the active part of the mode will be shown and will have the same legend, i.e., the solid part of the schematic curve of Fig. 12. Also, the intersection between the modes, i.e., the bimodal points, will be denoted by solid triangles as shown in the figure.

Fig. 13 shown the variation of the buckling coefficient, K, with the rotational restraint coefficient (Γ), for $\beta=1$, $\Psi=0.2$ and various degrees of lateral restraint ($\alpha=0$, 0.4, 0.8 and 1). The number in the brackets denotes the number of half-sine waves in the buckling mode. For free in-plane motion, (i.e., the solid curve), the plate buckles into a single half-sine wave for the pinned condition ($\Gamma=0$). Increasing Γ results in a rapid increase in the initial value of K. The plate buckling mode then changes to a full-sine wave at $\Gamma\approx23$. Beyond this value, the rate of increase gradually

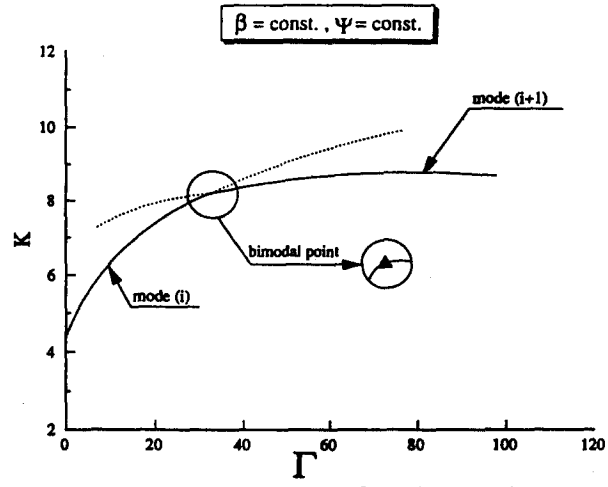

Fig. 12 Schematic of typical K-Γ curve for plate under stress gradient.

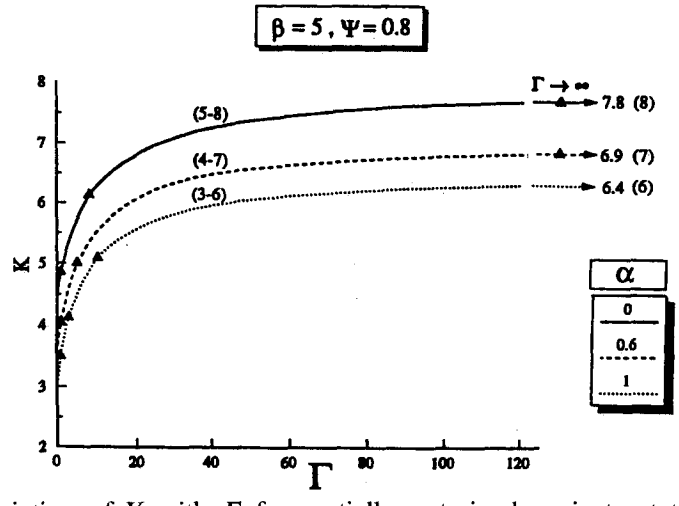

Fig. 13 Variation of K with Γ, for partially restrained against rotation condition, $\beta=1$, $\Psi=0.2$, α is variable.

diminishes as K becomes asymptotic to the clamped condition at $K=12.9$. For the laterally restrained conditions, i.e., $\alpha\neq0$, the K-Γ curves possess similar characteristics, (i.e., much of the increase in K occurs at the start of the curve). However, the magnitude of K decreases by increasing the lateral restrain intensity, α. This decrease can be measured by drawing a vertical line from a fixed value of Γ. The intersection of this decrease can be measured by drawing a vertical line from a fixed value of Γ. The intersection of this line with each curve gives the value of K for the given lateral restraint value. Note also that for this particular aspect ratio, unlike the free in-plane motion, $\alpha=0$, where the buckling mode changes from a half to a full sine wave, the plate maintains the half-sine wave buckling mode throughout the transition from pinned to clamped for all values of $\alpha\neq0$.

Fig. 14 shows the K-Γ curves for a larger aspect ratio, $\beta=5$, $\Psi=0.8$ and $\alpha=0.06$ and 1.

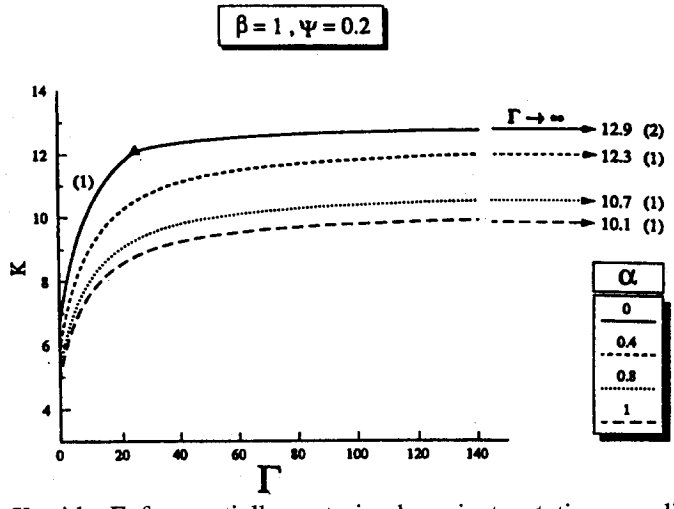

Fig. 14 Variation of K with Γ, for partially restrained against rotation condition, $\beta=5$, $\Psi=0.8$, α is variable.

The numbers in the brackets above each curve represent the active buckling mode changes throughout the entire range of pinned to clamped edges, (i.e., $\Gamma=0\rightarrow\infty$). For example, for the free translation case ($\alpha=0$), the plate buckles into five half-sine waves when it is pinned; the bucking mode then changes to three sine waves, or six half-sine waves when it is pinned; the buckling mode then changes to three sine waves, or six half-sine waves, at $\Gamma\approx1.2$, to seven half-sine waves at $\Gamma\approx8$ and finally to four sine-waves at $\Gamma\approx140$ and maintains this buckling mode to the clamped condition. The solid triangles on the arrows indicate that a change in the buckling mode occurs at values of Γ larger than 120. For the laterally restrained condition, beside the decrease in the K values, the initial and final buckling modes are different; for $\alpha=0.6$ the buckling mode changes from four to seven half-sine waves and for $\alpha=1$ from three to six half-sine waves. To give insight to the reduction in the buckling load and mode, if Γ is fixed at 10, the K value and number of half-sine waves for $\alpha=0$ are 6.29 and 7, respectively, for $\alpha=0.6$ are 5.53 and 6, and for $\alpha=1$ are 4.9 and 5. Note also the that the buckling modes change in the early stages of the K-Γ curve. This rapid change of the buckling mode was also observed for other cases studied as the plate aspect ratio increased.

4. Conclusions

The usual prediction of the buckling loads and associated buckling modes for plates under combined compression and in-plane bending ignores the lateral restraint imposed by the attached elements, (e.g. flange of I-section, web of box or channel section, ⋯ etc.). As a result of this restraint, however, a set of interactive forces come into play that destabilizes the plate resulting in a lower buckling load and possibly a different mode over the case of free edge translation. The normal forces, in this case, N_y, very linearly in the transverse direction equal $\alpha\nu N_1$ along the heavily loaded edge and $\alpha\nu\Psi N_1$ along the other. The difference in these forces is equilibrated by uniform shears, acting along the loaded edges, each of magnitude $0.5\alpha\nu\beta(1-\Psi)N_1$. The shear forces along the unloaded edges, on the other hand, varies linearly

and is of magnitude $-\alpha\nu\beta(1-\Psi)(\xi-0.5)N_1$. These forces are functions of the lateral restraints coefficient (α) which describes the freedom of the unloaded edges to move laterally and varies from 0 to 1, the stress gradient coefficient, Ψ, which causes the imbalance in the normal forces, N_y, and the plate aspect and Poisson's ratios. If the plate is considered as free to move, as if there were no attached restraints to this movement, the lateral coefficient equals zero and all these forces disappear. If the plate is in uniform compression, i.e., $\Psi=1$, all the shear forces disappear and the plate is under bi=axial compression.

The paper has investigated the influence of the lateral restraint on the buckling behaviour of non-uniformly compressed plates. The Galerkin method was used to perform the analysis. While the loaded edges were treated as simply supported, three boundary conditions for the unloaded edges were analyzed, simply supported, clamped and partially restrained against rotation. The numerical implementation was illustrated and various automation strategies, based on the properties of the resulting matrices, were suggested to economize on computation. Results were presented showing the variation of the buckling load and the associated buckling mode for the full range of lateral restraint, α, from edges free to move, $\alpha=0$, to fully restrained edges, $\alpha=1$, for various plate aspect ratios and stress gradient coefficients. The investigation showed the importance of defining the in-plane boundary condition in the buckling analysis of plates under this type of loading. A reduction up to 39% was obtained in some cases by changing the in-plane boundary condition from free to translate to fully restrained. Moreover, the buckling mode, which is an important quantity in estimating the pose-buckling reserve, was also changed.

Acknowledgements

The financial support provided to the author from the Natural Sciences and Engineering Council of Canada (NSERC) is gratefully acknowledged.

Notations

a	length of the plate
A_s	cross sectional area of the stiffeners
B	typical $(m\times n)\times(i\times j)$ matrix
b_{mnij}	entries of the B matrix
b	width of the plate
C	torsional rigidity of the stiffeners
D	plate bending rigidity per unit width, $=Et^3/12\ (1-\nu^2)$
E	elastic modulus
$H_m(\xi)$, $C_n(\eta)$	displacement functions
F_{mnij}, E_{mnij}, R_{mnij}, K_{mnij}	load matrices
K	buckling coefficient
m	number of half waves in the longitudinal direction
MF^1, MF^2	modification factors
N_x	compressive forces per unit length in the x direction
t	thickness of the plate
β	plate aspect ratio
Γ	torsional restraint coefficient
η	non-dimensional width, $=y/b$

ν	Possion ratio
ξ	non-dimensional length, $=x/a$; and
Ψ	stress gradient coefficient

References

Bedair, O. K. (1996), "Buckling behaviour of plates partially retrained aganinst rotation under stress gradient", *Int. J. Structural Engineering and Mechanics.* **4**(4), 383-396.

Bedair, O. K. (1996), "On the post-buckling behaviour of plates under stress gradient", *Int. J. Structural Engineering and Mechanics*, **4**(4), pp. 397-414.

Beedle, L. S. (ed.), (1991), *Stability of Metal Structures,* a World View, 2nd ed., Structural Stability Research Council, USA.

Bradford, M. A. (1989), "Buckling of longitudinally stiffened plates in bending and compression". *Can. J. Civ. Eng.* **16**, 607-614.

Bulson, P. S. (1967), "Local stability and strength of structural sections". *Thin Walled Structures,* Chatto & Windus, England 208-247.

Column Research Committee of Japan, (1971), *Handbook of Structural Stability* Corona Publishing Co., Tokyo.

Galambos, T. V. (1988), *Guide to Stability Design Criteria for Metal Structures,* 4th ed., Structural Stability Research Council, John Wiley & Sons, New York.

Gaylord, E. H. and Gaylord, C. N. (1990), *Structural Engineering Handbook,* McGraw-Hill, USA.

Johnson, J. H. and Noel, G. R. (1953), "Critical bending stress for flat rectangular plates supported along all edges and elastically restrained against rotation along the unloaded compression edge". *J. Aero. Sci.* **19**, 535-540.

Lau, S. C. W. and Hancock, G. J. (1986), "Buckling of thin flat-walled structures by a spline finite strip method". *Thin Walled Structures* **4**, 269-294.

Maeda, Y. and Okura, I. (1984), "Fatigue strength of plate girder in bending considering out-of-plane deformation of web" *Proc. JSCE, Structural Eng./Earthquake Eng.* **1**, 149-159.

Okura, I., Yen, B. T. and Fisher, J. W., (1993), "Fatigue of thin-walled plate girders". *Structural Engineering International* **1**, 39-44.

Rhodes, J. and Harvey, J. M. (1977), "Examination of plate post-buckling behaviour". *J. Engrg. Mech., ASCE.* **103**, 461-478.

Rhodes, J. and Harvey, J. M. (1976), "Plain channel section struts in compression and bending beyond the local buckling load". *Int. J. Mech. Sci.* **8**, 511-519.

Schuette, E. H. and McCulloch, J. C. (1947), "Charts for the minimum weight design of multiweb wings in bending", *NACA TN* 1323.

Usami, T. (1982), "Post-buckling of plates in compression and bending". *J. Struct. Div. ASCE.* **108**, 591-609.

Walker, A. C. (1968) "Maximum loads for eccentrically loaded thin-walled channel struts" *IABSE.* **28**, 169-181.

Walker, A. C. (1967), "Flat rectangular plates subjected to a linearly-varing edge compressive loading". *Thin Walled Structures,* Chatto & Windus, England 208-247.